International Journal of Hydrogen Energy
Volume 46, Issue 2, 6 January 2021, Pages 1615-1626

Insights on the ethanol oxidation reaction at electrodeposited PdNi catalysts under conditions of increased mass transport

Daniel Martín-Yerga [a, 1], Gunnar Henriksson [b], Ann Cornell [a]

https://doi.org/10.1016/j.ijhydene.2020.10.103

Insights on the ethanol oxidation reaction at electrodeposited PdNi catalysts under conditions of increased mass transport

Daniel Martín-Yerga[1*#], Gunnar Henriksson[2], Ann Cornell[1*]

[1]*Department of Chemical Engineering, KTH Royal Institute of Technology, SE-100 44 Stockholm, Sweden*

[2]*Department of Fibre and Polymer Technology, KTH Royal Institute of Technology, SE-100 44 Stockholm, Sweden*

Corresponding Author

* D. Martín-Yerga, daniel.martin-yerga@wawick.ac.uk

* A. Cornell, amco@kth.se

[#]***Current address:***

Department of Chemistry, University of Warwick, Gibbet Hill Rd, CV4 7AL Coventry, United Kingdom

Declarations of interest: None

ABSTRACT

The development of high-performance electrocatalysts for alcohol oxidation is still a major challenge to use these reactions for sustainable energy applications such as hydrogen production. In addition, understanding the reactivity under different hydrodynamic conditions is essential since the fuel is continuously fed to the anode in practical applications. In this work, the synthesis, characterization and electroactivity of bimetallic PdNi nanocoatings generated by electrodeposition toward the ethanol oxidation reaction (EOR) is described. A catalyst formed by $Pd_{0.91}Ni_{0.09}$ nanoflowers showed the highest EOR activity and enhanced performance under moderate mass transport rate. Both OH^- concentration and hydrodynamics affected the EOR activity and the product selectivity. Acetic acid was the main EOR product, but acetaldehyde formation increased when OH^- was limiting or under faster mass transport rates. This study provides novel knowledge to understand the EOR on PdNi catalysts and exposes the importance of evaluating hydrodynamic conditions when developing new electrocatalysts.

KEYWORDS: *Electrocatalysis; Ethanol oxidation reaction; Hydrodynamic effects; Product analysis; Binary catalysts.*

INTRODUCTION

Generation of sustainable energy remains one of the biggest challenges for realizing a future fossil fuel-free society.[1] Some alcohols can be produced from biomass, which is considered a renewable source of clean energy[2] and, accordingly, the oxidation of alcohols has attracted large interest in recent years.[3,4] Ethanol is a promising source in fuel cells for electricity generation[5,6] since it has higher energy density (about 8 kWh kg^{-1}) than hydrogen. Oxidation of alcohols could also become an important reaction for the sustainable production of hydrogen by electrolysis.[7] Previous studies[8] have shown that H_2 production by oxidation of ethanol could require around 20 kWh kg^{-1}, significantly lower than the 50 kWh kg^{-1} required by conventional water splitting. Valuable organic sub-products such as acetate may also be generated if the oxidation is not complete,[8,9] leading to a more sustainable process.

However, the low electrical energy consumption in these applications is only possible using specific electrocatalysts that allow the oxidation at low potentials. Pt-based materials have been widely employed as electrocatalysts for alcohol oxidation,[10,11] although Pd catalysts seem to show a higher activity for ethanol.[12,13] Latest developments on Pd electrocatalysts for the EOR include the use of nanoparticles with tunable high-index facets to control the catalytic activity[14] or catalyst reactivation steps to achieve high stability promoted by the beneficial properties of metal-oxide supports.[15] Nonetheless, the high cost of the pure metal and the typical deactivation issues [16,17] preventing to reach high current densities are still major obstacles for their application at a larger scale. One way to minimize these issues is the use of bimetallic materials.[18–20] Fabrication of these materials would typically require a lower amount of the noble metal (decreasing the catalyst cost), and the presence of specific metals such as Bi,[21] Ni[13] or Sn[12] has usually led to increased catalyst activity and stability, also supported by computational calculations.[22] Preparation of bimetallic catalysts with advanced structures leading to high surface area materials is one of the latest trends to improve the alcohol oxidation reactions. For instance, porous nanobowls,[23] or self-standing tremella-like superstructures[24] have recently been reported as excellent

Pd-based bimetallic catalysts for the EOR. Nickel has been one of the most popular materials to generate Pt or Pd bimetallic catalysts[18,25] as a result of its low cost and high stability in alkaline media. For instance, PdNi catalysts synthesized by hydrothermal methods have been previously demonstrated to facilitate the ethanol oxidation compared to monometallic Pd. [26–29] Electrodeposition seems to be more straightforward to prepare PdNi coatings than hydrothermal methods, while also showing good catalytic activity toward ethanol oxidation.[30,31] Previous studies using PdNi for the EOR have mainly focused on showing the positive influence of Ni addition on the electrochemical activity and finding optimal Pd:Ni ratios.[32] Consequently, there is a lack of general information about the role of different experimental conditions on the EOR performance using PdNi catalysts, and particularly, on the reaction mechanism and product selectivity.

In practical applications of alcohol oxidation such as fuel cells or electrolysis, the alcohol is continuously fed to the anode. Therefore, it is important to consider the hydrodynamic effects on the activity when designing and optimizing electrode structures, but this factor is usually neglected in many reported studies. Accordingly, there are important aspects regarding the mass transport in electrocatalytic reactions that are still not well understood, but have been lately shown to be relevant.[33,34] Recent reports have focused on understanding these effects by using rotating disk electrodes for alcohols such as methanol and ethanol on Pt-based catalysts.[34–37] Contradictory effects, largely attributed to the catalyst structure, have been reported for increased mass transport rate. Flat or thin-layer catalysts generally show decreased currents for the alcohol oxidation with increasing rotation rate, explained by the removal of intermediates by convection preventing a more complete oxidation.[34,37] However, a current increment with rotation rate was observed using thicker or nanoporous catalyst films.[37,38] This fact has been attributed to the trapping of reaction intermediates for longer times within the porous structure opening up the possibility for further oxidation, which adds up to the inherent performance enhancement usually observed for porous

catalysts.[39,40] A scheme illustrating the proposed effect of catalyst structure on the EOR pathways under increased mass transport conditions is shown in Figure 1. However, this hypothesis has not been proved so far by carrying out analysis of reaction products under different hydrodynamic conditions. In addition, most of these reports refer to alcohol oxidation on Pt-based catalysts in acidic media and, thus, the lack of understanding of mass transport effects is still more evident for Pd-based or bimetallic catalysts in alkaline media.

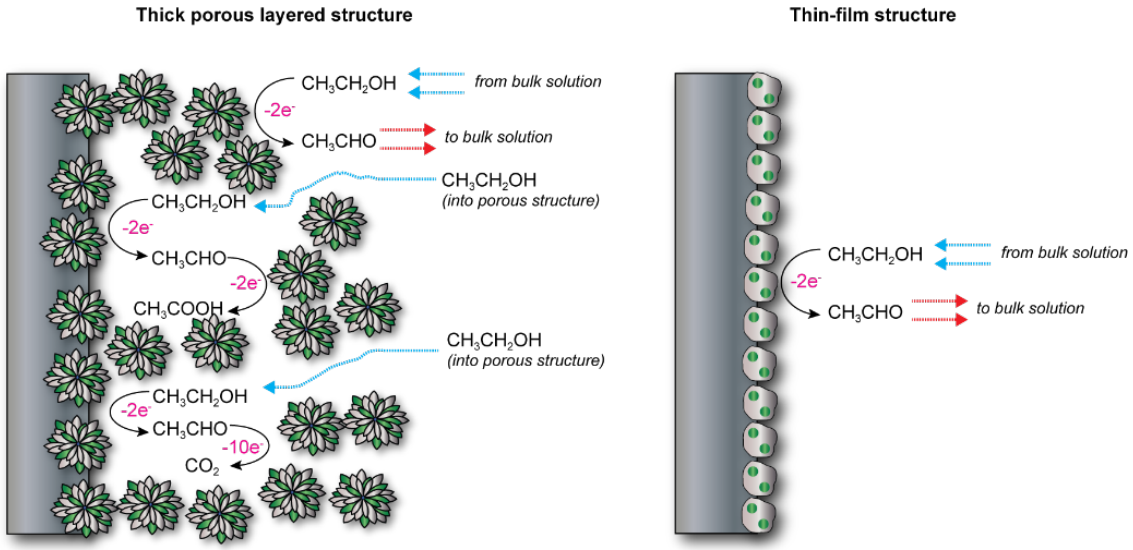

Figure 1. Scheme illustrating the possible differences on the ethanol oxidation reactions depending on the catalyst structure under conditions of increased mass transfer. Soluble products can stay within the catalyst porous structure for longer times enabling their further oxidation (left part) compared to their rapid transport to the bulk solution happening on thin-film catalysts (right part).

In this work, bimetallic PdNi electrocatalysts were prepared by a simple electrodeposition method and their response toward the ethanol oxidation reaction (EOR) was studied. The role of NaOH concentration, mass transport rate and catalyst structure on the EOR activity and mechanism was explored by recording iR-corrected polarization curves and analyzing the product distribution by High-Performance Liquid Chromatography (HPLC). This study provides significant novel findings on the EOR with PdNi catalysts

under different hydrodynamic conditions, revealing the mass transport rate and OH^- concentration as important factors in determining the EOR activity and product selectivity.

EXPERIMENTAL

Solutions and reagents

Nickel(II) nitrate hexahydrate, palladium(II) chloride (> 59.0% Pd; >99.9%, metal basis), sodium chloride, ethanol absolute, sodium hydroxide, acetaldehyde, acetic acid (glacial) and sulfuric acid (HPLC grade) were purchased from VWR (Radnor, PA, USA). Hydrochloric acid (37%) and Nafion solution (5% wt) were purchased from Sigma-Aldrich (St. Louis, MO, USA). Pt (20%) on carbon black (Vulcan XC-72) was obtained from De Nora. All reagents were of analytical grade. Ultrapure water obtained with a Millipore DirectQ3 purification system from Millipore (Burlignton, MA, USA) was used throughout this work. The electrodeposition solution was composed of 100 mM $Ni(NO_3)_2$ and 1 mM $PdCl_2$ in 0.3 M HCl and 0.5 M NaCl. Under these conditions, the main component of palladium is the $[PdCl_4]^{2-}$ complex.[41] For the monometallic Pd catalyst, the film was electrodeposited using the same solution but in the absence of the nickel salt. All the experiments of ethanol oxidation were performed in NaOH solutions in ultrapure water.

Electrocatalyst preparation

Electrodeposited PdNi films were prepared from the electrodeposition solution (25 mL) onto nickel disks with a geometric area of 1 cm^2. The disks were polished before each experiment using 1 μm polishing alumina and washed with ultrapure water in an ultrasonic bath. Galvanostatic electrodeposition was performed in a two-electrode glass cell with a carbon rod counter electrode by applying -50 mA cm^{-2} for 60 s. Different catalysts were prepared: A-PdNi, for which the electrodeposition was performed in a quiescent solution and B-PdNi and B-Pd, for which the electrodeposition was performed while the electrode was

rotating at 500 rpm (under increased mass transfer). B-Pd was prepared from a solution without nickel. After the deposition, the electrodes were rinsed with ultrapure water and used as prepared. A commercial 20% Pt/C catalyst was employed as reference catalyst. This catalyst was prepared by dispersing 2 mg of the catalyst powder in 0.5 mL of ultrapure water and 15 µL of Nafion solution (5% wt). The solution was sonicated for 15 minutes. Then, 10 µL of this dispersion was deposited on a glassy carbon electrode (geometric area of 0.126 cm^2) and dried under a N_2 atmosphere at room temperature.

Electrochemical measurements

Electrochemical measurements were performed using a PAR273A potentiostat/galvanostat from Ametek (Minneapolis, MN, USA). The electrode was rotated using an Ametek 616A instrument. Electrochemical measurements were conducted in a 100 mL glass three-electrode cell (50 mL when product analysis was performed) with a Pt mesh counter electrode and a Hg/HgO reference electrode (RE-A6P, Bio-Logic, 1 M NaOH). In order to obtain electrochemical information in absence of iR drop distortions at high current densities, iR-corrected polarization curves were recorded using the current-interrupt technique. The working electrode was polarized at the given current density and the current was interrupted. The decay of the potential was measured for 500 µs with a time resolution of 1 µs using a National Instrument cDAQ-9172 device. Nonlinear parameter fitting was applied to calculate the iR-corrected potential value, E(0), as previously discussed[42] using the following **equation 1**:

$$E(t) = E(0) - b \ln\left(1 + \frac{t\,j}{b\,C}\right) \quad \textbf{(1)}$$

where b is the Tafel slope, t is the time after the current interruption, j is the applied current density and C is the capacitance of the electrode. A typical current transient and a relationship obtained between the current and iR drop is shown in **Figure S1**. Current densities are presented considering the electrochemical surface area (ECSA). All measurements were performed at room temperature (21 ± 2 °C). Potentials were converted and are presented versus the reversible hydrogen electrode (RHE) using the **equation 2** (considering the pH of the NaOH aqueous solution).

$$E_{vs.\ RHE}\ (mV) = E_{vs.\ Hg/HgO} + 0.059\ pH + 0.140 \quad (\mathbf{2})$$

Physical characterization of catalysts

The morphology of the catalysts was imaged by scanning electron microscopy (SEM) on a JEOL JSM-7000F instrument at an acceleration voltage of 15 kV using a secondary electron detector unless stated otherwise. The elemental identification and quantification of the Pd/Ni ratio was carried out by Energy-dispersive X-ray spectroscopy (EDS) using the integrated detector of the SEM instrument. The crystalline properties of the catalysts were analyzed using powder X-Ray diffraction (XRD) recorded with a PANalytical PRO MPD diffractometer in Bragg-Brentano geometry with 1.5406 Å Cu Kα1 radiation, using a 2θ range of 38.0°-90.0° and a step size of 0.013°. The samples for EDS and XRD measurements were prepared by carefully scraping the catalyst layer from the electrode substrate. Inductively coupled plasma – atomic emission spectrometry (ICP-AES) using a Thermo Scientific ICAP 6500 instrument was employed to determine the Pd and Ni amount in the catalysts by analyzing the solution before and after the electrodeposition (**Table S1**).

Product analysis

Product analysis was carried out by HPLC on an Agilent 1260 Infinity II system with an Agilent Hi-Plex H column (250 x 4.6 mm) and refractive index detector (Agilent 1290 Infinity II RID) set on positive polarity. A sample volume of 10 µL was injected onto the column using the autosampler. Eluent was 5 mM HPLC-grade H_2SO_4 at a flowing rate of 0.4 mL min^{-1}. Column and detector temperature was 55 °C. A typical chromatogram for the EOR product analysis is shown in **Figure S2**.

RESULTS AND DISCUSSION

Physical characterization of the electrodeposited catalysts

Three different catalysts were fabricated by electrodeposition as mentioned in the Experimental section: a) with Pd/Ni in a quiescent solution, b) with Pd/Ni in solution while the electrode was rotating, and c) with only Pd in solution and the electrode rotating. For simplicity, these catalysts are named as A-PdNi, B-PdNi and B-Pd, respectively. **Figure 2** shows representative SEM images at the nanoscale (40000X magnification) where the morphology of the catalyst can be observed. **Figure 2a** shows that the A-PdNi catalyst is composed of quasi-spherical nanoparticles with a rough surface and diameters ranging from 60 to 100 nm. The B-PdNi catalyst (**Figure 2b**) is also formed by quasi-spherical nanoparticles but with morphological features resembling nanoflowers. The nanoflowers are significantly larger than the nanoparticles of the A-PdNi catalyst (around 150-300 nm) due to the further growth of the individual particles by the increased mass transfer to the electrode during deposition. In a previous work, where PdNi catalysts were prepared on Ni foam under similar experimental conditions,[43] the nanoflowers were formed by aggregation of smaller nanoparticles as determined by transmission electron microscopy (TEM) analysis. The B-PdNi catalyst was also formed by a thicker coating as demonstrated by the larger amount of electrodeposited metals determined by ICP-AES (Table S1) and visually observed as a darker coating. It seems clear that the hydrodynamic conditions during the electrodeposition have a strong effect on the morphology and size of nanoparticles, controlling its structure (see also **Figures S3 and S4** at higher and lower magnifications). **Figure 2c** shows the B-Pd catalyst, which consisted of rough Pd nanoparticles. These nanoparticles are also bigger (90-130 nm) than those of the A-PdNi catalyst but smaller than the nanoflowers of B-PdNi, proving that the simultaneous electrodeposition of Ni with Pd also affects the morphological structure of the catalysts.

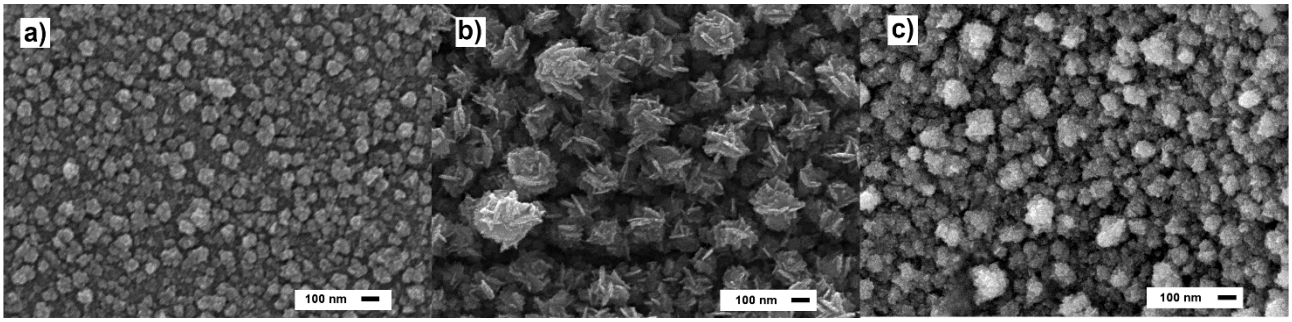

Figure 2. SEM images of the a) A-PdNi, b) B-PdNi and c) B-Pd catalysts. Scale bar is 100 nm.

EDS analysis was performed to confirm the presence of the metals in the bimetallic catalysts. **Figure S5** shows the EDS spectra for the A-PdNi, B-PdNi and B-Pd catalysts. Pd was found in all the spectra, which confirms its presence in the catalysts. Nickel was also found in the A-PdNi and B-PdNi catalysts with Pd:Ni atomic ratios of 72:27 (±5) and 91:9 (±2), respectively. The significant difference between the concentration ratio in the precursor solution (1:100, Pd:Ni) and the atomic ratio in the catalysts can be explained by thermodynamic and mass transfer effects during electrodeposition (see section S6 of the S.I. for discussion). The EDS spectrum for B-Pd (Figure S5c) confirmed that the catalyst was completely formed by this metal. XRD analysis (**Figure S6**) also suggested that the bimetallic catalysts are formed by a Pd/Ni alloy material.

Surface electrochemistry of electrodeposited catalysts

The electrochemical surface area (ECSA) of Pd catalysts can be obtained by evaluating their surface electrochemistry. Cyclic voltammetry experiments between 0.2 and 1.2 V (vs RHE) were performed in a N_2-saturated 1 M NaOH solution. **Figure S7** shows the cyclic voltammograms for the three different Pd catalysts. The anodic and cathodic peaks observed around 0.3 V are assigned to the adsorption/desorption of hydrogen on Pd atoms.[44] OH^- ions are also adsorbed on the Pd atoms during the anodic sweep (**equation 3**), a process usually assigned[45] to the small voltammetric peak observed at a potential close to

+0.6 V. Pd oxidation also takes place according to **equation 4** at higher electrode potentials, for which the previous OH^- adsorption plays a crucial role.[46]

$$Pd + OH^- \rightarrow Pd - OH_{ads} + e^- \quad \textbf{(3)}$$

$$Pd - OH_{ads} + OH^- \rightarrow Pd - O + H_2O + e^- \quad \textbf{(4)}$$

The cathodic sweep shows the reduction of the palladium oxide (+0.77 V) formed during the anodic sweep. If the potential limit is around +1.2 V, the cathodic peak can be assigned to the reduction of a monolayer of palladium oxide.[47] The charge under the peak (Q) can be correlated with the ECSA according to **equation 5**, assuming that the reduction of a monolayer[48] takes 0.405 mC cm^{-2}.

$$ECSA\ (cm^2) = {}^{Q\ (mC)}/_{0.405\ mC\ cm^{-2}} \quad \textbf{(5)}$$

The estimated roughness factors (R_f = ECSA/geometric area) were 7.8 (±0.7), 12.2 (±1.0) and 10.1 (±0.8) for the A-PdNi, B-PdNi and B-Pd, respectively. These roughness factors are similar to those previously reported for PdNi catalysts (R_f = 0.5-22) prepared by single-step electrodeposition,[30,49] being only smaller than those obtained for very porous materials (R_f = 10-100) but prepared by complex time-consuming multi-step procedures.[49] The ECSA of the B-PdNi is enhanced compared to the other catalysts which could be due to the special morphological features of the catalyst as observed by SEM. The ECSA (1.09 cm^2, roughness factor 8.65) for the commercial Pt/C catalyst was calculated by integrating the H_2 desorption peaks in 0.1 M H_2SO_4 following the standard method widely described in the literature.[50]

Electrocatalytic oxidation of ethanol under different hydrodynamic conditions

Catalysts activity toward ethanol electrooxidation was evaluated in alkaline solution (1 M ethanol, 0.1 M NaOH). The mass transport (electrode rotation) affected significantly the EOR response as recorded by cyclic voltammetry (**Figure 3**), with 800 rpm as the optimal rotation rate for the B-PdNi catalyst. Accordingly, further experiments were carried out in a quiescent solution and under the optimal mass transport

rate (electrode rotating at 800 rpm) in order to evaluate the different catalysts and reaction conditions under two different hydrodynamic scenarios. **Figure 4** shows the iR-corrected polarization curves for all the catalysts in both hydrodynamic conditions. A process can be discerned at very low current densities, which is assigned to catalyst surface reactions by comparison with the polarization curves obtained for the blank solution (**Figure S8**), and since the potential is still too low for the onset of the EOR. The linear region observed at around 0.5 V (vs RHE) is attributed to ethanol oxidation on Pd active sites, as demonstrated by the EOR onset in the voltammetric responses (**Figure S9**). The B-PdNi catalyst reached higher current densities for this region as a result of a higher EOR activity. Other processes occurring at more positive potentials (> +1.4 V), particularly for the A-PdNi catalyst, with a larger atomic ratio in nickel than the B-PdNi catalyst, may be related to oxygen evolution or ethanol oxidation on nickel, [20] which may also be possible as shown in **Figure S10**. As seen in Figure 4 under increased mass transport conditions (electrode rotating at 800 rpm), the polarization curves for the B-PdNi, B-Pd and Pt catalysts shifted toward higher current densities, likely due to the increased amount of reactants arriving to the electrode surface. The B-PdNi catalyst also showed the highest EOR activity under increased mass transport conditions reaching a current density of 5.6 mA cm^{-2} (normalized by ECSA). However, a significant shift toward lower current densities was obtained for the EOR on the A-PdNi catalyst, indicating that this catalyst with a thinner and less porous surface compared to B-PdNi has lower activity under these increased mass-transport conditions. Similar effects have been previously found for the ethanol and methanol oxidation reactions using Pt-based catalysts,[33,34,51] and the catalyst structure seems to govern the specific behavior (current increase or decrease).[37] Removal of a soluble intermediate such as acetaldehyde from the electrode surface has been proposed as the cause of the current decrease by preventing the posterior oxidation to acetate or CO_2, [37] but to our knowledge this hypothesis has not been confirmed by product analysis so far in RDE experiments. This behavior has been observed for flat or thin-film electrodes where the removal of soluble species is efficient and seems to be the case for the A-PdNi catalyst. This catalyst

coating is thinner than the other catalysts as demonstrated by the smaller amount of electrodeposited material (Table S1), and its electrochemical behavior seems to be similar to previously reported thin-film catalysts.[37] Not only did the B-PdNi catalyst showed higher activity but it was also more stable in long-term experiments. **Figure S11** shows the chronoamperometric response obtained during 8 h for the different Pd-based catalysts at +0.9 V in 1 M ethanol in 0.1 M NaOH, where the B-PdNi catalyst kept a higher current density throughout the experiment.

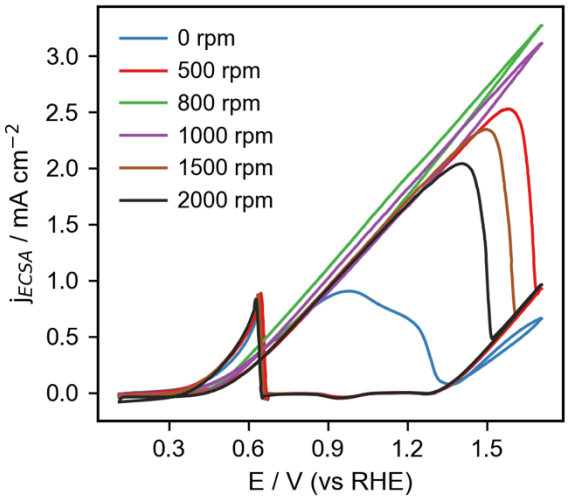

Figure 3. Cyclic voltammograms for 1 M ethanol in 0.1 M NaOH at several rotation rates (0, 500, 800, 1000, 1500, 2000 rpm) using the B-PdNi catalyst. Scan rate was 10 mV s^{-1}.

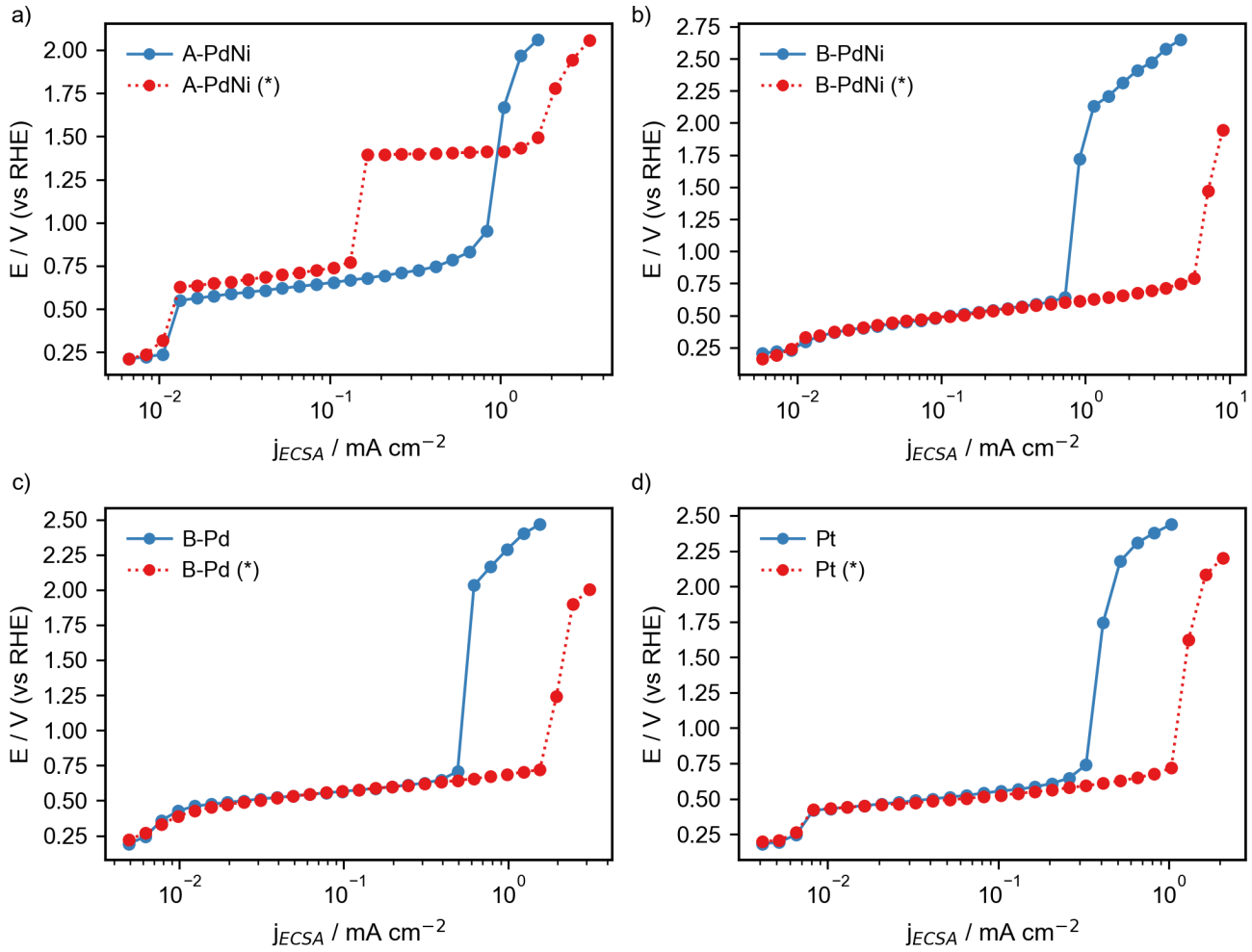

Figure 4. iR-corrected polarization curves normalized by the ECSA for the ethanol oxidation reaction (1 M in 0.1 M NaOH) obtained using the different electrocatalysts: a) A-PdNi, b) B-PdNi, c) B-Pd and d) Pt. (*) indicates that the experiment was performed under increased mass transfer conditions (electrode was rotated at 800 rpm).

Effect of ethanol and hydroxide concentrations on the EOR under different hydrodynamic conditions

It is well known that hydroxide ions play an important role on the EOR mechanism and could influence the reaction pathway and rate,[52] but they also contribute to the formation of stable Pd oxides (equation 4) that deactivate surface sites. OH^- ions are involved on the EOR independently of the generated reaction

283 product but the pathway to CO_2 or acetic acid requires a larger amount of OH^- compared to acetaldehyde,
284 according to the EOR chemical **equations 6-8**:

285 $$CH_3CH_2OH + 2\,OH^- \rightarrow CH_3CHO + 2\,H_2O + 2\,e^- \quad (\mathbf{6})$$

286 $$CH_3CH_2OH + 4\,OH^- \rightarrow CH_3COOH + 3\,H_2O + 4\,e^- \quad (\mathbf{7})$$

287 $$CH_3CH_2OH + 12\,OH^- \rightarrow 2\,CO_2 + 9\,H_2O + 12\,e^- \quad (\mathbf{8})$$

288 To evaluate the effect of the OH^- concentration, iR-corrected polarization curves were also recorded under
289 quiescent and increased mass transport conditions for 1 M ethanol solution in 1 M NaOH (**Figure 5**). A
290 significant shift toward higher current densities was observed in a quiescent solution compared to the
291 results obtained in 0.1 M NaOH (Figure 4) for all the catalysts. This fact confirms that OH^- is strongly
292 involved in the EOR. A higher OH^- concentration was also positive for the EOR onset potential as can be
293 observed in this region of the voltammetric response (**Figure S12**). A positive effect on the current densi-
294 ties for the B-PdNi, B-Pd and Pt catalysts was also observed under increased mass transport conditions
295 (Figure 5, dashed red lines), but the enhancement was significantly smaller than that observed for 0.1 M
296 NaOH. This fact implies that the OH^- concentration is a limiting factor at large ethanol/OH^- concentration
297 ratios, which is mitigated by regenerating the electrode interface with new OH^- molecules coming from
298 the bulk solution. A lower activity in terms of current densities and potentials was found for the A-PdNi
299 catalyst under increased mass transport rate, indicating more complex relations than a simple limiting
300 OH- concentration.

301

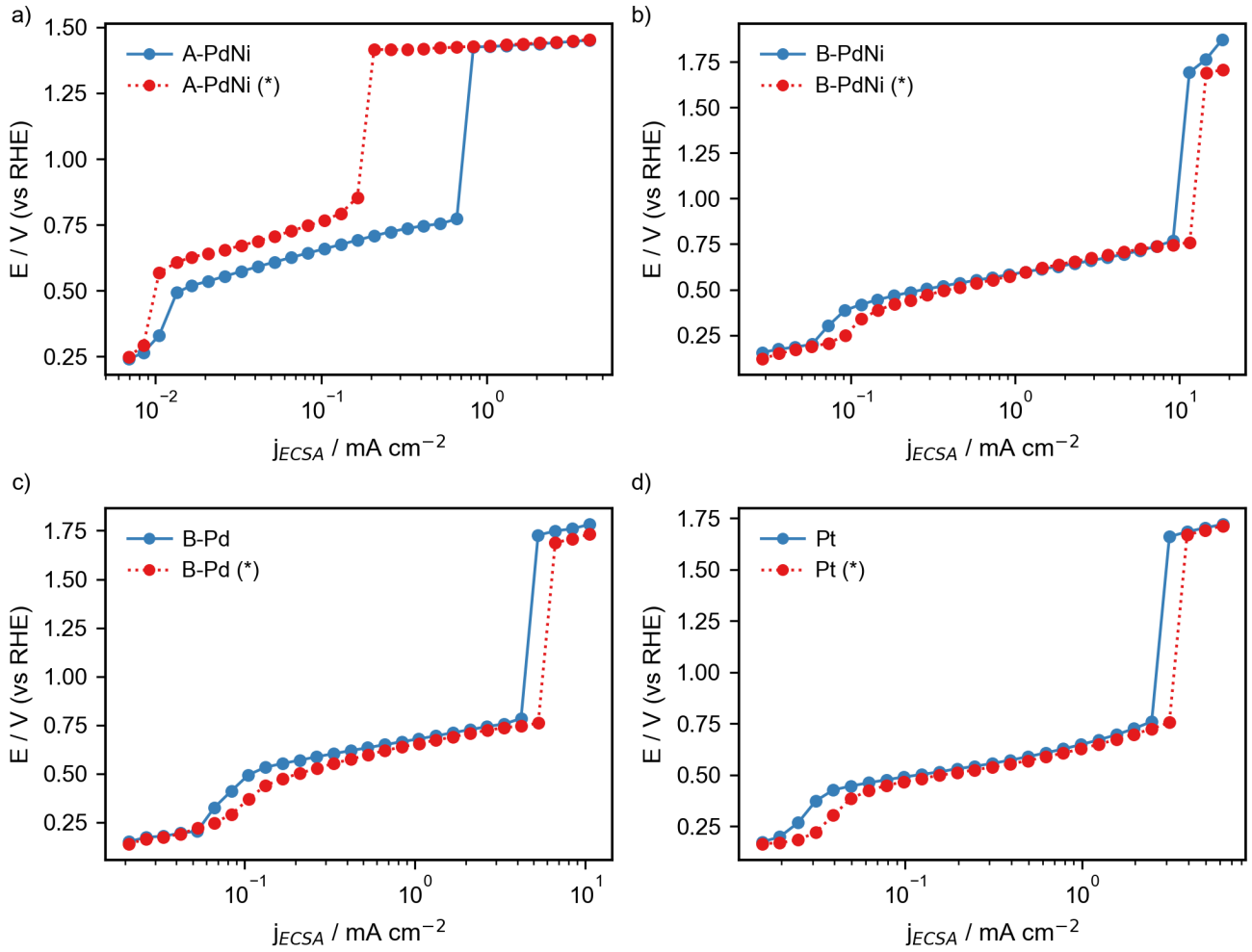

Figure 5. iR-corrected polarization curves normalized by the ECSA for the ethanol oxidation reaction (1 M in 1 M NaOH) obtained using the different electrocatalysts: a) A-PdNi, b) B-PdNi, c) B-Pd and d) Pt. (*) indicates that the experiment was performed under increased mass transfer conditions (electrode was rotated at 800 rpm).

A more systematic study of the OH^- concentration effect was carried out for the most active catalyst (B-PdNi). **Figure 6** shows the polarization curves recorded in a quiescent solution for 1 M ethanol and increasing NaOH concentrations (0.1, 0.5, 1 and 2 M). A clear trend of increasing current densities with increasing NaOH concentrations up to 1 M was obtained, further demonstrating that the reaction rate is strongly limited by the OH^- concentration, in agreement with the EOR chemical equations 6-8. A similar

trend in the current densities was observed under increased mass transport conditions also up to 1 M NaOH, suggesting that even if the mass transport of OH^- is more efficient than in a quiescent solution some limitation still exists at low OH^- concentration, which is mitigated by increasing it. Interestingly, the current densities reached in 2 M NaOH under these conditions were smaller than those obtained in 1 M NaOH. This fact might be a result of catalyst deactivation by PdO formation [17] occurring faster at high OH^- concentrations, [53] but the difference is relatively small to draw any conclusions and further studies focusing on high OH^- concentrations would be interesting to elucidate this deactivation phenomenon.

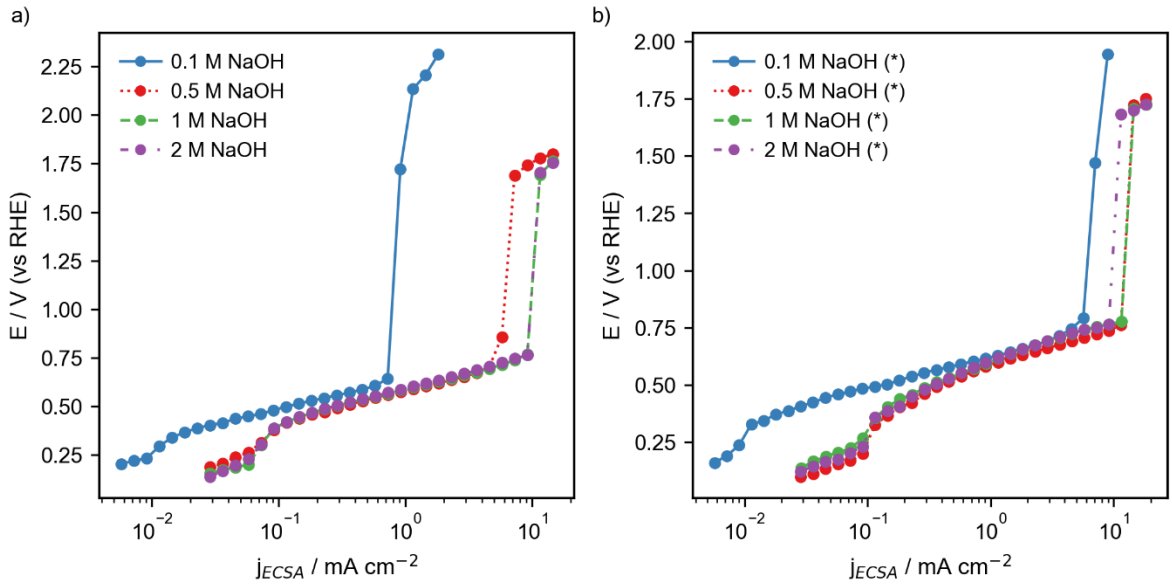

Figure 6. iR-corrected polarization curves obtained for different concentrations of NaOH (0.1, 0.5, 1 and 2 M) with 1 M ethanol using the B-PdNi catalyst in a quiescent solution (a) and with the electrode rotating at 800 rpm (b).

Polarization curves were also recorded at a higher ethanol concentration (3 M) in 1 M NaOH (**Figure 7**) in order to evaluate if the current densities could be increased from the limit observed at 1 M ethanol in 1 M NaOH. Under a quiescent solution, the polarization curve reached a similar current density for the EOR as for 1 M ethanol, which agrees with OH^- concentration still being the limiting factor. An enhanced EOR response was observed under increased mass transport conditions for 3 M ethanol, reaching an ECSA-

normalized current density of 21.7 mA cm^{-2} (~265 mA cm^{-2}, geometric). These results indicate that the OH^- limiting factor can also be overcome at higher ethanol concentrations when increased mass transfer conditions are employed.

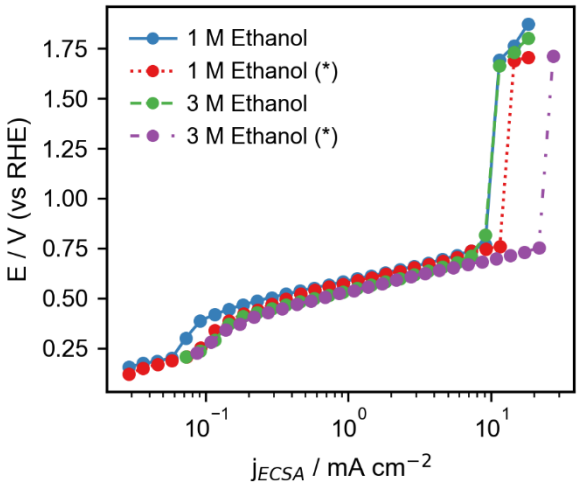

Figure 7. iR-corrected polarization curves obtained for different concentrations of ethanol (1 M and 3 M) in 1 M NaOH using the B-PdNi catalyst. "*" indicates that the experiment was performed with the electrode rotating at 800 rpm (increased mass transfer rate).

Catalysts performance at high current densities

To test the viability of the EOR catalysts under the high current densities expected to be used in industrial applications, iR-corrected measurements at 100 mA cm^{-2} (geometric area) were recorded using a solution of 3 M ethanol in 1 M NaOH and electrode rotating at 800 rpm. **Figure 8** shows the galvanostatic curves obtained for the different catalysts during the EOR. It is readily observed that most of the catalysts were quickly deactivated at these high current densities, demonstrated by a significant potential shift to high potentials where water oxidation may happen. However, the B-PdNi catalyst was able to keep a low potential (around +0.7 V) during all the experiment (at least for 30 min). These results agree with the previous experiments, where a higher activity was observed for the B-PdNi particularly under increased mass

transport conditions. A substantial generation of H_2 bubbles was also observed at the cathode during the experiment, demonstrating the possibility of H_2 production at a good rate and low potentials.

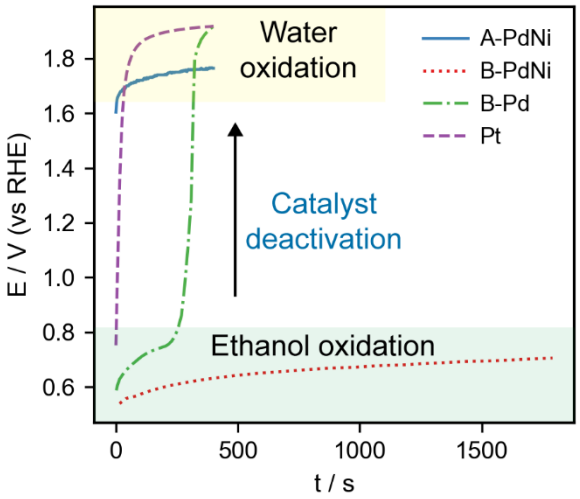

Figure 8. iR-corrected galvanostatic curves recorded at 100 mA cm^{-2} (*geometric area*) using the different catalysts in a 3 M ethanol + 1 M NaOH solution under conditions of increased mass transfer rate (electrode rotated at 800 rpm).

EOR product analysis under different conditions

The previous experiments have shown that the EOR can be limited by the mass transport of OH^- to the electrode surface. In order to evaluate this effect on the EOR mechanism, the product distribution for different ethanol/NaOH concentration ratios was analyzed by HPLC. Galvanostatic experiments (+7.5 mA cm^{-2} for 3h) were carried out using the B-PdNi catalyst for the oxidation of 1 M ethanol in 0.1 M and 1 M NaOH. A quiescent solution was employed in order to keep the OH^- concentration as a limiting factor near the electrode surface. **Figure 9a** shows the product distribution for both experiments, where acetic acid and acetaldehyde were the only detected reaction products, as also previously reported with Pd-based catalysts.[54,55] It is worth to mention that some aldehydes tend to form aldol condensation products in

alkaline media,[56] but additional peaks were not observed by HPLC in reaction samples or even in standard acetaldehyde solutions, also in agreement to previous works.[55] A significantly higher selectivity toward acetaldehyde was obtained in 0.1 M NaOH compared to 1 M NaOH: 29.5% vs. 3.6%, although the main product in both cases was still acetic acid. These results agree with OH^- being involved on the EOR, and particularly affecting the acetic acid formation since a larger amount of OH^- is required to generate this product in contrast to acetaldehyde (see EOR chemical equations 6-8). The EOR could happen by two different pathways on noble metal electrocatalysts [37,46,52,57] as shown in **Figure 10**. In the C1-pathway, the C-C carbon bond is broken leading to CO_2 (CO_3^{2-} in alkaline media) as the final product. However, this pathway is difficult to achieve at low temperatures [58] because the cleavage of the C-C is challenging and, therefore, its contribution to the total current is usually low. [59] Since the Faradaic efficiencies obtained in the galvanostatic experiments were close to 100% (99.9% and 95% for 0.1 M and 1 M NaOH, respectively), it is reasonable to discard a significant contribution of the C1-pathway under these conditions. Thus, the mechanism under the experimental conditions in this work likely follows the C2-pathway,[60] where the C-C bond remains intact during the oxidation. Ethanol is firstly converted to acetaldehyde by a two-electron transfer and eventually to acetate by another two-electron transfer. This pathway may be initiated by the adsorption of ethanol on the active sites, usually as adsorbed ethoxy species in alkaline media.[61] Then, a dehydrogenation step leads to the generation of acetaldehyde. Acetaldehyde can diffuse to the bulk solution and be a final product of the reaction or if it stays close to the electrode, it could be converted to acetate in a second oxidation step (see **Figure S13** for acetaldehyde oxidation on B-PdNi). For the latter reaction, oxygenated species need to be supplied, which agrees with the increment of acetaldehyde to acetate conversion with higher pH in these experiments and as previously observed. [52]

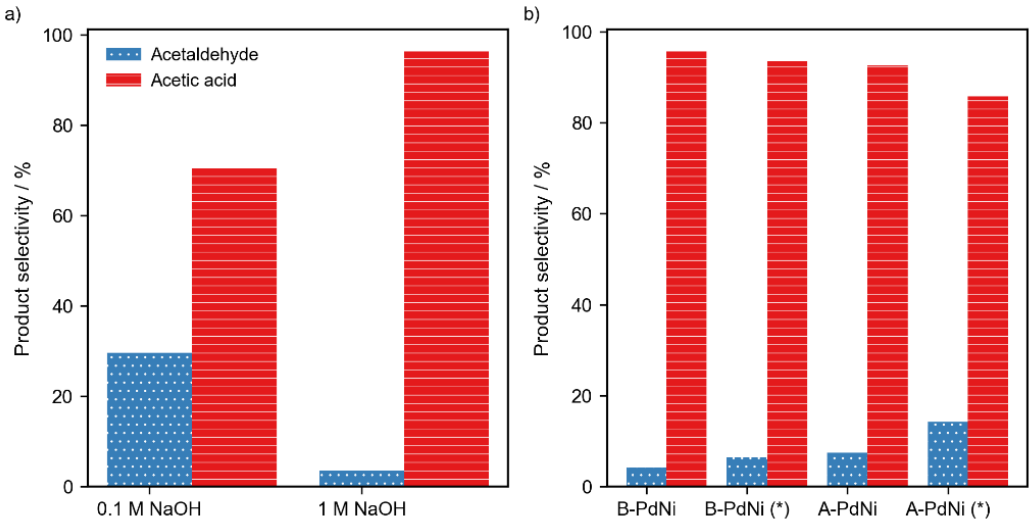

385

386 **Figure 9**. EOR product selectivity after performing the reaction under different conditions. a) B-PdNi catalyst,
387 quiescent solution, 1 M Ethanol, 0.1 vs 1 M NaOH. b) A-PdNi vs B-PdNi catalysts; 1 M Ethanol in 1 M NaOH,
388 "*" indicates that the experiment was performed with the electrode rotating at 800 rpm.

389

390

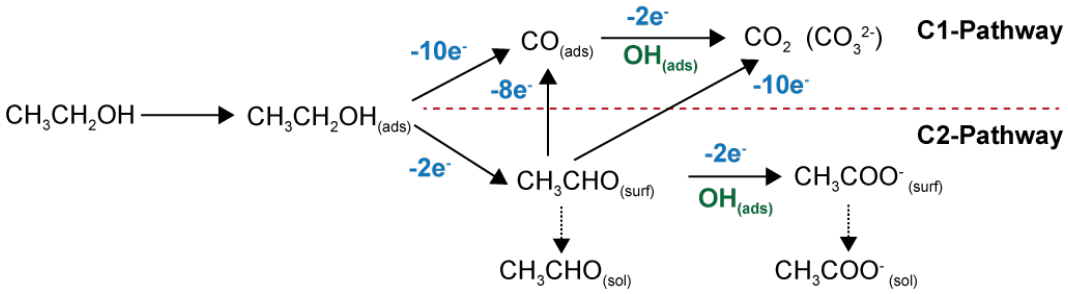

391

392 **Figure 10.** Simplified mechanism pathways for the electrochemical oxidation of ethanol on noble metals.[37]

393

394 The EOR product distribution might also be affected by different hydrodynamic conditions. As previously
395 reported [37] and observed in this work, catalysts with different structure (i.e. thickness/porosity) show a
396 different behavior under increased mass transport rate. A change in the product distribution has been pro-
397 posed as a possible cause (Figure 1), but that hypothesis has not been confirmed by carrying out product
398 analysis so far. The EOR product distribution was evaluated with two catalysts, A-PdNi and B-PdNi,

399 which showed a different behavior under increased mass transport conditions, typical of thin-film or
400 thick/porous catalysts, respectively. Galvanostatic experiments for 1 M ethanol in 1 M NaOH were rec-
401 orded under a quiescent solution and increased mass transport rate (electrode rotating at 800 rpm), and
402 the product distribution was analyzed by HPLC (**Figure 9b**). Galvanostatic conditions were chosen to
403 keep a similar oxidation potential for both catalysts: 1 mA cm^{-2} for A-PdNi, and 10 mA cm^{-2} for B-PdNi
404 (geometric current densities). In all cases, the main product was acetic acid. An increment in the selectivity
405 toward acetaldehyde was observed under increased mass transport conditions: from 4.3% to 6.5% for the
406 B-PdNi catalyst and from 7.5% to 14.2% for the A-PdNi catalyst. Faradaic efficiencies were in the range
407 of 94-98%, which rules out a significant formation of CO_2. These results generally agree with the hypoth-
408 esis that the lower EOR activity on thin-film catalysts under increased mass transport conditions may
409 come from a decrease in the formation of higher oxidation state products, and enhanced formation of
410 soluble intermediates such as acetaldehyde, while thicker catalysts seem to be able to keep forming higher
411 oxidation state products such as acetic acid. However, the main product in both hydrodynamic conditions
412 was still acetic acid, suggesting that acetaldehyde oxidation happens quickly after its formation near the
413 electrode surface. It is worth to mention that the different atomic composition between B-PdNi and A-
414 PdNi catalysts may also have some influence on the EOR reactivity, and therefore, a more systematic
415 study using catalysts with more controlled thickness/porosity and composition would be interesting to
416 elucidate the effect of both factors on the EOR under increased mass transport rate.
417

418 **CONCLUSIONS**

419 A catalyst formed by PdNi nanoflowers with special morphological and electrocatalytic properties was
420 prepared by a simple one-step electrodeposition method. This catalyst showed a high activity toward the
421 EOR, particularly under optimum hydrodynamics, which was found to be at a moderate rotation rate (800
422 rpm). This high-activity catalyst enabled the EOR at a low potential (~0.7 V) at 100 mA cm^{-2} and low

temperature. OH^- concentration was found to be a limiting factor for the EOR, especially toward the formation of acetic acid, which was the main product detected by HPLC. Acetaldehyde formation could be enhanced at limiting OH^- concentrations or under increased mass transport conditions, demonstrating the importance of these parameters to direct the reaction. In addition, higher acetaldehyde formation was also observed using a thinner PdNi catalyst, which might be due to a facilitated release of intermediates to the bulk solution when the catalyst has this structure. More systematic studies to confirm this behavior using catalysts with controlled structure could be very valuable. In summary, this work highlights the importance of the hydrodynamic conditions on the EOR activity and mechanism, and further understanding this process may boost the design of effective catalysts for alcohols oxidation in practical applications where the fuel is continuously fed to the anode.

ACKNOWLEDGMENTS

We would like to thank Dr. Jekabs Grins and Dr. Kjell Jansson from Stockholm University for their help with the XRD and SEM measurements. We gratefully acknowledge support from the Swedish Energy Agency (Project 44666-1) and the Swedish Foundation for Strategic Research (SSF) through grant number EM16-0010.

REFERENCES

[1] S. Chu, A. Majumdar, Opportunities and challenges for a sustainable energy future, Nature. 488 (2012) 294–303. https://doi.org/10.1038/nature11475.

[2] J. Goldemberg, Ethanol for a Sustainable Energy Future, Science (80-.). 315 (2007) 808–810. https://doi.org/10.1126/science.1137013.

[3] S. Wasmus, A. Küver, Methanol oxidation and direct methanol fuel cells: a selective review, J. Electroanal. Chem. 461 (1999) 14–31. https://doi.org/10.1016/S0022-0728(98)00197-1.

[4] R. Rizo, R.M. Arán-Ais, E. Padgett, D.A. Muller, M.J. Lázaro, J. Solla-Gullón, J.M. Feliu, E. Pastor, H.D. Abruña, Pt-Rich core /Sn-Rich subsurface /Pt skin Nanocubes As Highly Active and Stable Electrocatalysts for the Ethanol Oxidation Reaction, J. Am. Chem. Soc. 140 (2018) 3791–3797. https://doi.org/10.1021/jacs.8b00588.

[5] E. Antolini, Catalysts for direct ethanol fuel cells, J. Power Sources. 170 (2007) 1–12. https://doi.org/10.1016/j.jpowsour.2007.04.009.

[6] C. Bianchini, P.K. Shen, Palladium-Based Electrocatalysts for Alcohol Oxidation in Half Cells and in Direct

Alcohol Fuel Cells, Chem. Rev. 109 (2009) 4183–4206. https://doi.org/10.1021/cr9000995.
[7] C. Coutanceau, S. Baranton, Electrochemical conversion of alcohols for hydrogen production: a short overview, Wiley Interdiscip. Rev. Energy Environ. 5 (2016) 388–400. https://doi.org/10.1002/wene.193.
[8] V. Bambagioni, M. Bevilacqua, C. Bianchini, J. Filippi, A. Lavacchi, A. Marchionni, F. Vizza, P.K. Shen, Self-Sustainable Production of Hydrogen, Chemicals, and Energy from Renewable Alcohols by Electrocatalysis, ChemSusChem. 3 (2010) 851–855. https://doi.org/10.1002/cssc.201000103.
[9] Y. Holade, C. Morais, K. Servat, T.W. Napporn, K.B. Kokoh, Toward the Electrochemical Valorization of Glycerol: Fourier Transform Infrared Spectroscopic and Chromatographic Studies, ACS Catal. 3 (2013) 2403–2411. https://doi.org/10.1021/cs400559d.
[10] Y. Kwon, Y. Birdja, I. Spanos, P. Rodriguez, M.T.M. Koper, Highly Selective Electro-Oxidation of Glycerol to Dihydroxyacetone on Platinum in the Presence of Bismuth, ACS Catal. 2 (2012) 759–764. https://doi.org/10.1021/cs200599g.
[11] H.E.M. Hussein, H. Amari, J. V. Macpherson, Electrochemical Synthesis of Nanoporous Platinum Nanoparticles Using Laser Pulse Heating: Application to Methanol Oxidation, ACS Catal. 7 (2017) 7388–7398. https://doi.org/10.1021/acscatal.7b02701.
[12] W. Du, K.E. Mackenzie, D.F. Milano, N.A. Deskins, D. Su, X. Teng, Palladium–Tin Alloyed Catalysts for the Ethanol Oxidation Reaction in an Alkaline Medium, ACS Catal. 2 (2012) 287–297. https://doi.org/10.1021/cs2005955.
[13] R. Jiang, D.T. Tran, J.P. McClure, D. Chu, A Class of (Pd–Ni–P) Electrocatalysts for the Ethanol Oxidation Reaction in Alkaline Media, ACS Catal. 4 (2014) 2577–2586. https://doi.org/10.1021/cs500462z.
[14] N.-F. Yu, N. Tian, Z.-Y. Zhou, T. Sheng, W.-F. Lin, J.-Y. Ye, S. Liu, H.-B. Ma, S.-G. Sun, Pd Nanocrystals with Continuously Tunable High-Index Facets as a Model Nanocatalyst, ACS Catal. 9 (2019) 3144–3152. https://doi.org/10.1021/acscatal.8b04741.
[15] X. Wu, J. He, M. Zhang, Z. Liu, S. Zhang, Y. Zhao, T. Li, F. Zhang, Z. Peng, N. Cheng, J. Zhang, X. Wen, Y. Xie, H. Tian, L. Cao, L. Bi, Y. Du, H. Zhang, J. Cheng, X. An, Y. Lei, H. Shen, J. Gan, X. Zu, S. Li, L. Qiao, Binary Pd/amorphous-SrRuO3 hybrid film for high stability and fast activity recovery ethanol oxidation electrocatalysis, Nano Energy. 67 (2020) 104247. https://doi.org/10.1016/j.nanoen.2019.104247.
[16] J. Xie, P. Duan, N. Kaylor, K. Yin, B. Huang, K. Schmidt-Rohr, R.J. Davis, Deactivation of Supported Pt Catalysts during Alcohol Oxidation Elucidated by Spectroscopic and Kinetic Analyses, ACS Catal. 7 (2017) 6745–6756. https://doi.org/10.1021/acscatal.7b02201.
[17] L. Wang, A. Lavacchi, M. Bellini, F. D'Acapito, F. Di Benedetto, M. Innocenti, H.A. Miller, G. Montegrossi, C. Zafferoni, F. Vizza, Deactivation of Palladium Electrocatalysts for Alcohols Oxidation in Basic Electrolytes, Electrochim. Acta. 177 (2015) 100–106. https://doi.org/10.1016/j.electacta.2015.02.026.
[18] C. Zhu, D. Wen, M. Oschatz, M. Holzschuh, W. Liu, A.-K. Herrmann, F. Simon, S. Kaskel, A. Eychmüller, Kinetically Controlled Synthesis of PdNi Bimetallic Porous Nanostructures with Enhanced Electrocatalytic Activity, Small. 11 (2015) 1430–1434. https://doi.org/10.1002/smll.201401432.
[19] A.C. Queiroz, W.O. Silva, I.A. Rodrigues, F.H.B. Lima, Identification of bimetallic electrocatalysts for ethanol and acetaldehyde oxidation: Probing C2-pathway and activity for hydrogen oxidation for indirect hydrogen fuel cells, Appl. Catal. B Environ. 160–161 (2014) 423–435. https://doi.org/10.1016/j.apcatb.2014.05.055.
[20] D. Martín-Yerga, G. Henriksson, A. Cornell, Effects of Incorporated Iron or Cobalt on the Ethanol Oxidation Activity of Nickel (Oxy)Hydroxides in Alkaline Media, Electrocatalysis. 10 (2019) 489–498. https://doi.org/10.1007/s12678-019-00531-8.
[21] J. González-Cobos, S. Baranton, C. Coutanceau, Development of Bismuth-Modified PtPd Nanocatalysts for the Electrochemical Reforming of Polyols into Hydrogen and Value-Added Chemicals, ChemElectroChem. 3 (2016) 1694–1704. https://doi.org/10.1002/celc.201600147.
[22] B. Miao, Z.-P. Wu, M. Zhang, Y. Chen, L. Wang, Role of Ni in Bimetallic PdNi Catalysts for Ethanol Oxidation Reaction, J. Phys. Chem. C. 122 (2018) 22448–22459. https://doi.org/10.1021/acs.jpcc.8b05812.
[23] Z. Li, Y. Chen, G. Fu, Y. Chen, D. Sun, J.-M. Lee, Y. Tang, Porous PdRh nanobowls: facile synthesis and activity for alkaline ethanol oxidation, Nanoscale. 11 (2019) 2974–2980. https://doi.org/10.1039/C8NR09482A.
[24] F. Gao, Y. Zhang, F. Ren, Y. Shiraishi, Y. Du, Universal Surfactant-Free Strategy for Self-Standing 3D Tremella-Like Pd–M (M = Ag, Pb, and Au) Nanosheets for Superior Alcohols Electrocatalysis, Adv. Funct.

Mater. 30 (2020) 2000255. https://doi.org/10.1002/adfm.202000255.
[25] R.M. Altarawneh, T.M. Brueckner, B. Chen, P.G. Pickup, Product distributions and efficiencies for ethanol oxidation at PtNi octahedra, J. Power Sources. 400 (2018) 369–376. https://doi.org/10.1016/j.jpowsour.2018.08.052.
[26] Z. Qi, H. Geng, X. Wang, C. Zhao, H. Ji, C. Zhang, J. Xu, Z. Zhang, Novel nanocrystalline PdNi alloy catalyst for methanol and ethanol electro-oxidation in alkaline media, J. Power Sources. 196 (2011) 5823–5828. https://doi.org/10.1016/j.jpowsour.2011.02.083.
[27] R. Li, H. Mao, J. Zhang, T. Huang, A. Yu, Rapid synthesis of porous Pd and PdNi catalysts using hydrogen bubble dynamic template and their enhanced catalytic performance for methanol electrooxidation, J. Power Sources. 241 (2013) 660–667. https://doi.org/10.1016/j.jpowsour.2013.05.032.
[28] Y. Feng, D. Bin, B. Yan, Y. Du, T. Majima, W. Zhou, Porous bimetallic PdNi catalyst with high electrocatalytic activity for ethanol electrooxidation, J. Colloid Interface Sci. 493 (2017) 190–197. https://doi.org/10.1016/j.jcis.2017.01.035.
[29] X. He, L. Ning, A. Zhu, Q. Zhang, Q. Liu, Hollow nanoporous NiPd catalysts with enhanced performance for ethanol electro-oxidation, Int. J. Hydrogen Energy. 42 (2017) 24989–25000. https://doi.org/10.1016/j.ijhydene.2017.08.104.
[30] J.D. Lović, V.D. Jović, Electrodeposited Pd and PdNi coatings as electrodes for the electrochemical oxidation of ethanol in alkaline media, J. Solid State Electrochem. 21 (2017) 2433–2441. https://doi.org/10.1007/s10008-017-3595-2.
[31] J.D. Lović, V. Jović, Electrochemical behavior of electrodeposited Pd and PdNi coatings for the ethanol oxidation reaction in alkaline solution, J. Electrochem. Sci. Eng. 0 (2017). https://doi.org/10.5599/jese.445.
[32] T.S. Almeida, Y. Yu, A.R. de Andrade, H.D. Abruña, Employing iron and nickel to enhance ethanol oxidation of Pd-based anodes in alkaline medium, Electrochim. Acta. 295 (2019) 751–758. https://doi.org/10.1016/j.electacta.2018.10.187.
[33] F. Seland, R. Tunold, D.A. Harrington, Activating and deactivating mass transport effects in methanol and formic acid oxidation on platinum electrodes, Electrochim. Acta. 55 (2010) 3384–3391. https://doi.org/10.1016/j.electacta.2010.01.040.
[34] A. Bach Delpeuch, M. Jacquot, M. Chatenet, C. Cremers, The influence of mass-transport conditions on the ethanol oxidation reaction (EOR) mechanism of Pt/C electrocatalysts, Phys. Chem. Chem. Phys. 18 (2016) 25169–25175. https://doi.org/10.1039/C6CP04294E.
[35] A. Sayadi, P.G. Pickup, Evaluation of methanol oxidation catalysts by rotating disc voltammetry, Electrochim. Acta. 199 (2016) 12–17. https://doi.org/10.1016/j.electacta.2016.03.112.
[36] A. Sayadi, P.G. Pickup, Evaluation of ethanol oxidation catalysts by rotating disc voltammetry, Electrochim. Acta. 215 (2016) 84–92. https://doi.org/10.1016/j.electacta.2016.08.097.
[37] V.K. Puthiyapura, W.-F. Lin, A.E. Russell, D.J.L. Brett, C. Hardacre, Effect of Mass Transport on the Electrochemical Oxidation of Alcohols Over Electrodeposited Film and Carbon-Supported Pt Electrodes, Top. Catal. 61 (2018) 240–253. https://doi.org/10.1007/s11244-018-0893-6.
[38] J.R. Hayes, D. Zeller, C. Friesen, The Influence of Platinum Surface Morphology on the Electrooxidation of Methanol in Alkaline Solutions, in: ECS Trans., ECS, 2008: pp. 41–54. https://doi.org/10.1149/1.3010875.
[39] Y. Ouyang, H. Cao, H. Wu, D. Wu, F. Wang, X. Fan, W. Yuan, M. He, L.Y. Zhang, C.M. Li, Tuning Pt-skinned PtAg nanotubes in nanoscales to efficiently modify electronic structure for boosting performance of methanol electrooxidation, Appl. Catal. B Environ. 265 (2020) 118606. https://doi.org/10.1016/j.apcatb.2020.118606.
[40] L.Y. Zhang, Y. Ouyang, S. Wang, Y. Gong, M. Jiang, W. Yuan, C.M. Li, Ultrafast synthesis of uniform 4–5 atoms-thin layered tremella-like Pd nanostructure with extremely large electrochemically active surface area for formic acid oxidation, J. Power Sources. 447 (2020) 227248. https://doi.org/10.1016/j.jpowsour.2019.227248.
[41] J.M. van Middlesworth, S.A. Wood, The stability of palladium(II) hydroxide and hydroxy–chloride complexes: an experimental solubility study at 25–85°C and 1 bar, Geochim. Cosmochim. Acta. 63 (1999) 1751–1765. https://doi.org/10.1016/S0016-7037(99)00058-7.
[42] B. Endrődi, S. Sandin, V. Smulders, N. Simic, M. Wildlock, G. Mul, B.T. Mei, A. Cornell, Towards sustainable chlorate production: The effect of permanganate addition on current efficiency, J. Clean. Prod.

182 (2018) 529–537. https://doi.org/10.1016/j.jclepro.2018.02.071.
[43] D. Martín-Yerga, X. Yu, I. Terekhina, G. Henriksson, A. Cornell, In situ catalyst reactivation for enhancing alcohol electro-oxidation and coupled hydrogen generation, Chem. Commun. 56 (2020) 4011–4014. https://doi.org/10.1039/D0CC01321H.
[44] X. Niu, H. Zhao, M. Lan, Palladium deposits spontaneously grown on nickel foam for electro-catalyzing methanol oxidation: Effect of precursors, J. Power Sources. 306 (2016) 361–368. https://doi.org/10.1016/j.jpowsour.2015.12.044.
[45] C.-C. Hu, T.-C. Wen, Voltammetric investigation of palladium oxides—I: Their formation/reduction in NaOH, Electrochim. Acta. 40 (1995) 495–503. https://doi.org/10.1016/0013-4686(94)00324-T.
[46] Z.X. Liang, T.S. Zhao, J.B. Xu, L.D. Zhu, Mechanism study of the ethanol oxidation reaction on palladium in alkaline media, Electrochim. Acta. 54 (2009) 2203–2208. https://doi.org/10.1016/j.electacta.2008.10.034.
[47] M.D. Obradović, Z.M. Stančić, U.Č. Lačnjevac, V.V. Radmilović, A. Gavrilović-Wohlmuther, V.R. Radmilović, S.L. Gojković, Electrochemical oxidation of ethanol on palladium-nickel nanocatalyst in alkaline media, Appl. Catal. B Environ. 189 (2016) 110–118. https://doi.org/10.1016/j.apcatb.2016.02.039.
[48] K. Zhang, D. Bin, B. Yang, C. Wang, F. Ren, Y. Du, Ru-assisted synthesis of Pd/Ru nanodendrites with high activity for ethanol electrooxidation, Nanoscale. 7 (2015) 12445–12451. https://doi.org/10.1039/C5NR02713F.
[49] L. Mattarozzi, S. Cattarin, N. Comisso, R. Gerbasi, P. Guerriero, M. Musiani, L. Vázquez-Gómez, Preparation of compact and porous Pd-Ni alloys and study of their performances for ethanol oxidation in alkali, Electrochim. Acta. 307 (2019) 503–511. https://doi.org/10.1016/j.electacta.2019.03.219.
[50] M. Łukaszewski, Electrochemical Methods of Real Surface Area Determination of Noble Metal Electrodes – an Overview, Int. J. Electrochem. Sci. 11 (2016) 4442–4469. https://doi.org/10.20964/2016.06.71.
[51] F. Seland, C.E.L. Foss, R. Tunold, D. Harrington, Increasing and Decreasing Mass Transport Effects in the Oxidation of Small Organic Molecules, ECS Trans. 28 (2010) 203–210. https://doi.org/10.1149/1.3502351.
[52] S.C.S. Lai, S.E.F. Kleijn, F.T.Z. Öztürk, V.C. van Rees Vellinga, J. Koning, P. Rodriguez, M.T.M. Koper, Effects of electrolyte pH and composition on the ethanol electro-oxidation reaction, Catal. Today. 154 (2010) 92–104. https://doi.org/10.1016/j.cattod.2010.01.060.
[53] P.V.B. Santiago, R.A.G. Oliveira, J.M. Roquetto, N. Akiba, I. Gaubeur, C.A. Angelucci, J. Souza-Garcia, J.M. Feliu, Oxide formation as probe to investigate the competition between water and alcohol molecules for OH species adsorbed on platinum, Electrochim. Acta. 317 (2019) 694–700. https://doi.org/10.1016/j.electacta.2019.06.037.
[54] S.Y. Shen, T.S. Zhao, Q.X. Wu, Product analysis of the ethanol oxidation reaction on palladium-based catalysts in an anion-exchange membrane fuel cell environment, Int. J. Hydrogen Energy. 37 (2012) 575–582. https://doi.org/10.1016/j.ijhydene.2011.09.077.
[55] A. Santasalo-Aarnio, Y. Kwon, E. Ahlberg, K. Kontturi, T. Kallio, M.T.M. Koper, Comparison of methanol, ethanol and iso-propanol oxidation on Pt and Pd electrodes in alkaline media studied by HPLC, Electrochem. Commun. 13 (2011) 466–469. https://doi.org/10.1016/j.elecom.2011.02.022.
[56] J.B. Anderson, M.S. Peters, Acetaldehyde Aldol Condensation Kinetics., J. Chem. Eng. Data. 5 (1960) 359–364. https://doi.org/10.1021/je60007a033.
[57] S.C.S. Lai, M.T.M. Koper, Electro-oxidation of ethanol and acetaldehyde on platinum single-crystal electrodes, Faraday Discuss. 140 (2009) 399–416. https://doi.org/10.1039/B803711F.
[58] S. Sun, M.C. Halseid, M. Heinen, Z. Jusys, R.J. Behm, Ethanol electrooxidation on a carbon-supported Pt catalyst at elevated temperature and pressure: A high-temperature/high-pressure DEMS study, J. Power Sources. 190 (2009) 2–13. https://doi.org/10.1016/j.jpowsour.2009.01.073.
[59] G.A. Camara, T. Iwasita, Parallel pathways of ethanol oxidation: The effect of ethanol concentration, J. Electroanal. Chem. 578 (2005) 315–321. https://doi.org/10.1016/j.jelechem.2005.01.013.
[60] C. Busó-Rogero, E. Herrero, J.M. Feliu, Ethanol Oxidation on Pt Single-Crystal Electrodes: Surface-Structure Effects in Alkaline Medium, ChemPhysChem. 15 (2014) 2019–2028. https://doi.org/10.1002/cphc.201402044.
[61] T. Iwasita, E. Pastor, A dems and FTir spectroscopic investigation of adsorbed ethanol on polycrystalline platinum, Electrochim. Acta. 39 (1994) 531–537. https://doi.org/10.1016/0013-4686(94)80097-9.

SUPPLEMENTARY INFORMATION

Insights on the ethanol oxidation reaction at electrodeposited PdNi catalysts under conditions of increased mass transport

Daniel Martín-Yerga[1*#], Gunnar Henriksson[2], Ann Cornell[1*]

[1]Department of Chemical Engineering, KTH Royal Institute of Technology, SE-100 44 Stockholm, Sweden

[2]Department of Fibre and Polymer Technology, KTH Royal Institute of Technology, SE-100 44 Stockholm, Sweden

Corresponding Author

* D. Martín-Yerga, daniel-martin-yerga@warwick.ac.uk

* A. Cornell, amco@kth.se

[#]***Current address:***

Department of Chemistry, University of Warwick, Gibbet Hill Rd, CV4 7AL Coventry, United Kingdom

TABLE OF CONTENTS

S1. Amount of electrodeposited metals

Table S1. Amount of Pd and Ni (in mg) found on the electrodeposited catalysts by ICP-AES.

Catalyst	Pd (mg)	Ni (mg)	Atomic ratio (Pd:Ni)
A-PdNi	0.048 ± 0.006	0.008 ± 0.001	77:23
B-PdNi	0.18 ± 0.03	0.012 ± 0.002	89:11
B-Pd	0.22 ± 0.02	-	

S2. Current-interrupt transient

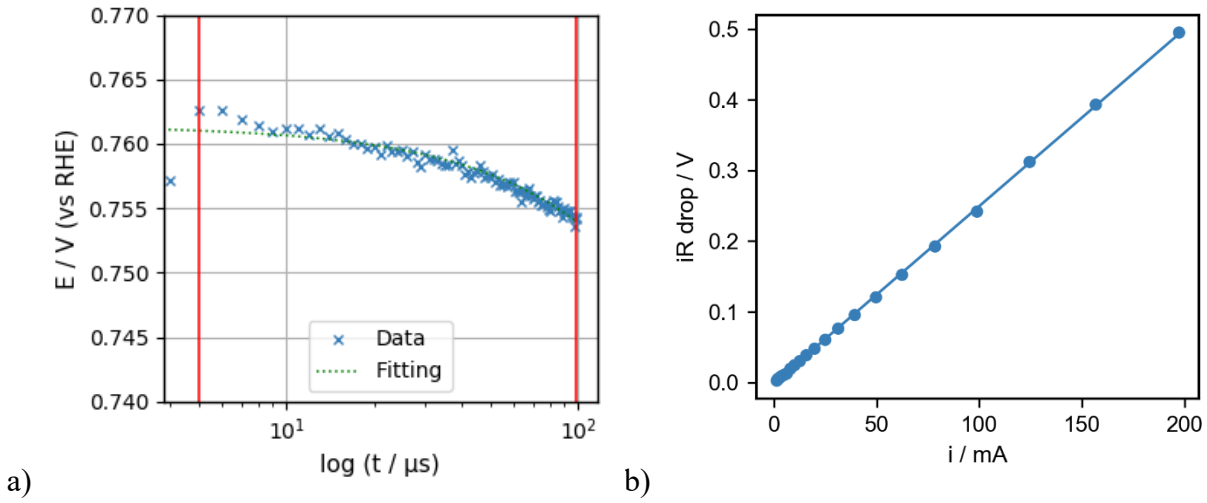

Figure S1. a) A typical fitted transient (recorded at j = 9.4 mA cm^{-2}, ECSA) using the B-PdNi catalyst in 1 M ethanol + 1 M NaOH while the electrode was rotating at 800 rpm. Fitting was performed between 5 and 100 µs (first points after the current interruptions showed significant deviation and were omitted from the fitting). b) Relationship between the current and the iR drop obtained from the current-interrupt experiments using the B-PdNi catalyst in 1 M ethanol + 1 M NaOH while the electrode was rotating at 800 rpm. Estimated uncompensated resistance was 2.51 Ω.

S3. HPLC chromatogram for ethanol oxidation products

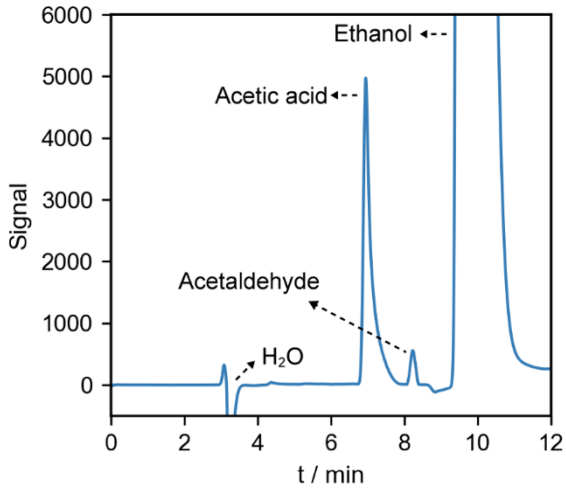

Figure S2. Typical HPLC chromatogram obtained after analyzing the resulting sample from oxidation of 1 M ethanol in 1 M NaOH using a B-PdNi catalyst (electrode rotating at 800 rpm). Identification of products was achieved by comparing the retention times of standard solutions of individual species.

S4. Scanning electron microscopy for PdNi catalysts at different magnifications

a) 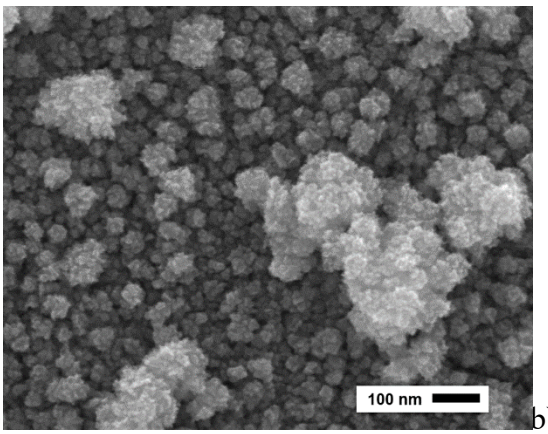

b) 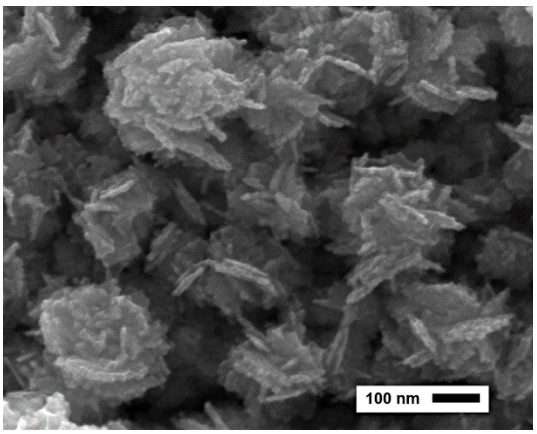

Figure S3. Scanning electron microscopy images of the A-PdNi (a) and B-PdNi (b) catalysts at higher magnification. The nanoflower shape is only observed for the B-PdNi and the A-PdNi catalyst seems to be formed by agglomeration of rough nanoparticles even for the biggest particles. B-PdNi image also shows a less compacted structure leading to a catalyst film with bigger pores. Scale bar is 100 nm.

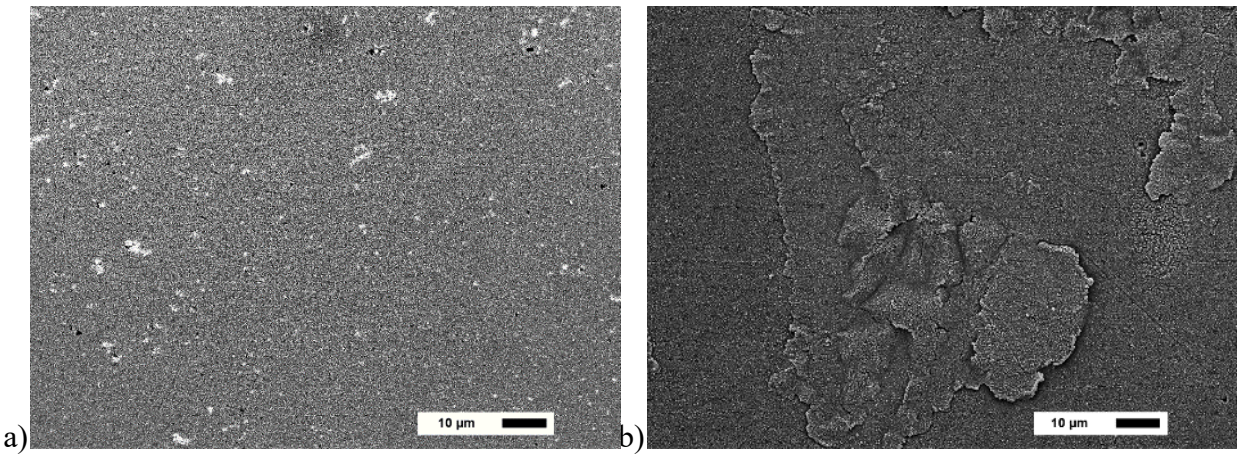

Figure S4. Scanning electron microscopy images of the A-PdNi (a) and B-PdNi (b) catalysts at lower magnification. Scale bar is 10 µm.

S5. Energy-dispersive X-ray spectra for the different Pd-based catalysts

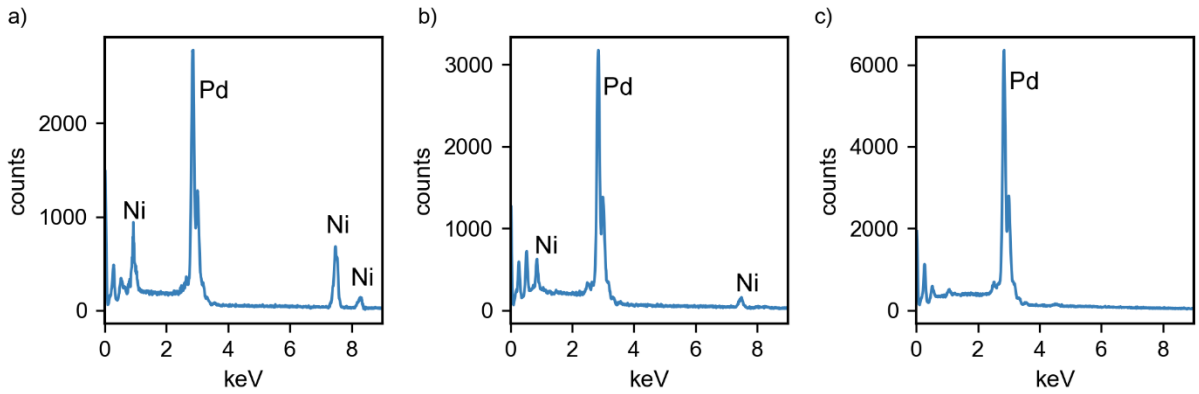

Figure S5. Energy-dispersive X-ray spectra obtained for the a) A-PdNi, b) B-PdNi and c) B-Pd catalysts.

S6. Insights on the catalyst electrodeposition

A strong difference between the concentration ratio in solution (1:100, Pd:Ni) and the atomic ratio in the catalysts was obtained. This may be explained by the fact that the reduction of $[PdCl_4]^{2-}$ is thermodynamically favored over the Ni^{2+} reduction.[1] These results also show that the mass transport conditions during the electrodeposition influences the atomic ratio of the catalysts. If mass transfer is slower (static solution, A-PdNi catalyst), $[PdCl_4]^{2-}$ is quickly reduced and depleted from the electrode surface, having to diffuse from the bulk solution. As the depletion of Ni^{2+} from the electrode surface would take more time, the catalyst is enriched with Ni. If the mass transfer rate is higher (rotating electrode, B-PdNi catalyst), the electrode/solution interface is quickly renewed with new reactants and thermodynamics has a higher influence on the electrodeposition: Pd(II) is reduced more easily than Ni(II) and the catalyst is enriched in Pd. Therefore, control of the mass transfer rate during the electrodeposition could be an interesting method to obtain electrocatalysts with tunable metallic ratios even using the same initial solution.

S7. X-ray diffraction patterns for the different Pd-based catalysts

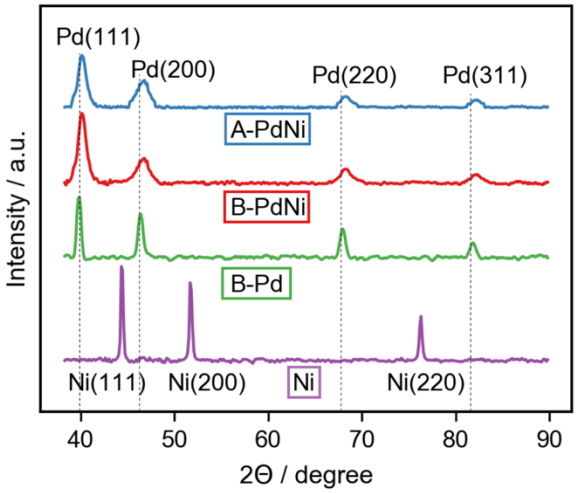

Figure S6. X-ray diffraction patterns for the three catalysts and electrodeposited nickel. Dashed lines represent the peak positions according to JCPDS No. 46-1043 card for the fcc Pd structure.

For the B-Pd catalyst, which is only composed by Pd, several peaks were observed at 2Θ values of 39.92, 46.44, 67.93 and 81.85°. These peaks are ascribed to the (111), (200), (220) and (311) lattice planes of pure fcc structure (JCPDS No. 46-1043).[2] For the bimetallic catalysts, the 2Θ values were slightly shifted with values of 40.22, 46.81, 68.27 and 82.36°, respectively, but they can also be assigned to the same lattice planes. However, no significant differences were found between the XRD patterns of the A-PdNi and B-PdNi catalysts. The peaks of the Pd crystalline facets were wider for both PdNi catalysts in comparison to the monometallic material (B-Pd catalyst). This fact may suggest that the material has an increased structural disorder or tensile stress,[3] suggesting that the material is forming a metallic alloy. The shift of the 2Θ peaks for the Pd crystalline facets in the PdNi catalysts also supports that the Pd lattice structure shrank after alloying with Ni (smaller atomic size than Pd). For instance, the d-spacing values calculated for the (111) planes were 2.241 and 2.258 Å for the PdNi and B-Pd catalysts, respectively. The pattern of pure electrodeposited Ni (in absence of Pd) is also shown in the figure. This material gave three peaks at 44.35, 51.68 and 76.30° assigned to the (111), (200) and (220) facets of Ni (JCPDS No. 04-0850).[2] However, they were not observed for the PdNi catalysts, which also agrees with the complete alloying of the bimetallic materials.

S8. Cyclic voltammograms for blank solution (1 M NaOH)

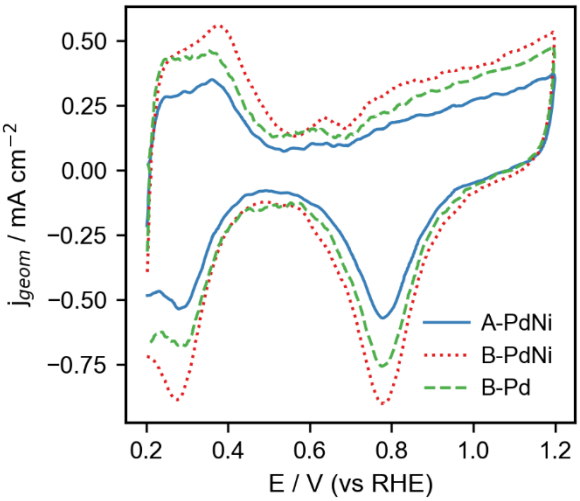

Figure S7. Cyclic voltammograms obtained in N_2-saturated 1 M NaOH with the three Pd-based catalysts. Scan rate was 25 mV s^{-1}. Potentials are referred to the RHE.

S9. iR-corrected polarization curves for blank solution (0.1 M NaOH)

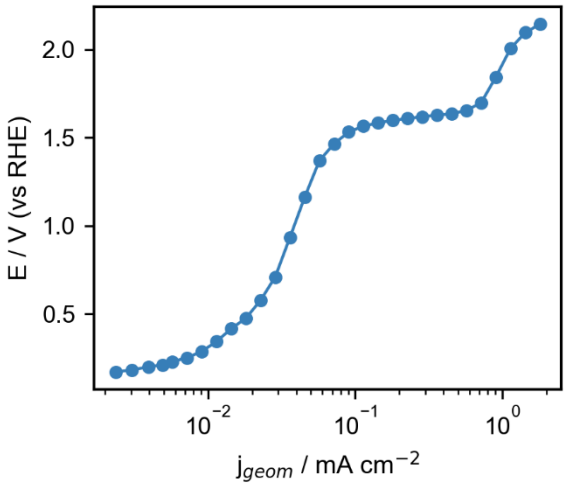

Figure S8. iR-corrected polarization curve recorded for the B-PdNi in a 0.1 M NaOH solution (quiescent conditions).

S10. Voltammetric onset of 1 M ethanol oxidation in 0.1 M NaOH

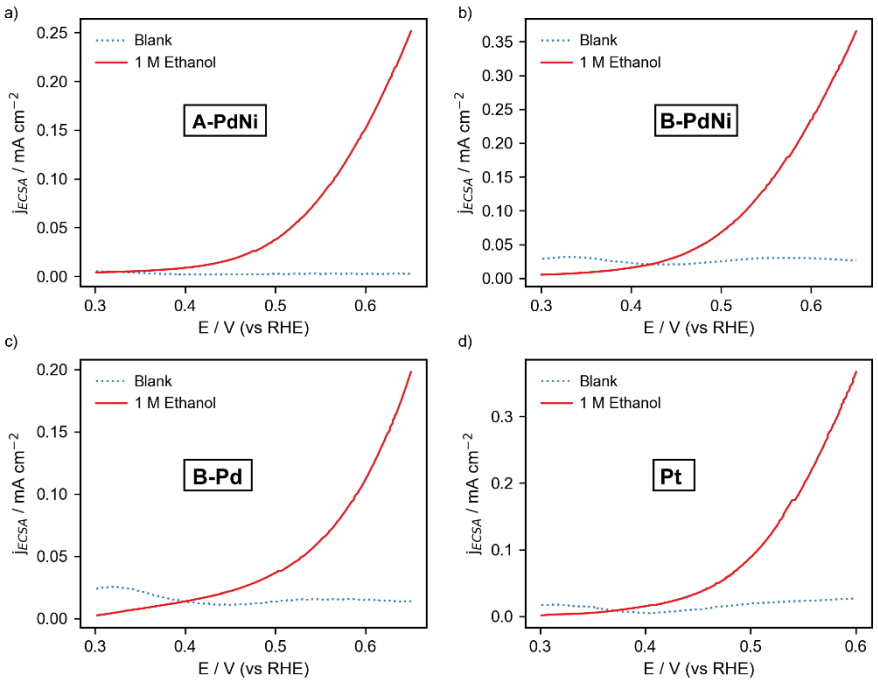

Figure S9. Voltammetric response normalized by the ECSA for the ethanol oxidation reaction (1 M in 0.1 M NaOH) using the different catalysts in a quiescent solution. Scan rate was 10 mV s^{-1}. Dashed blue line represent the response obtained for a blank solution (0.1 M NaOH). Since a significant iR drop distortion was observed at higher current densities, only the onset of the voltammetric process is shown where the iR drop is negligible and responses can be compared.

S11. Ethanol oxidation reaction on nickel catalyst

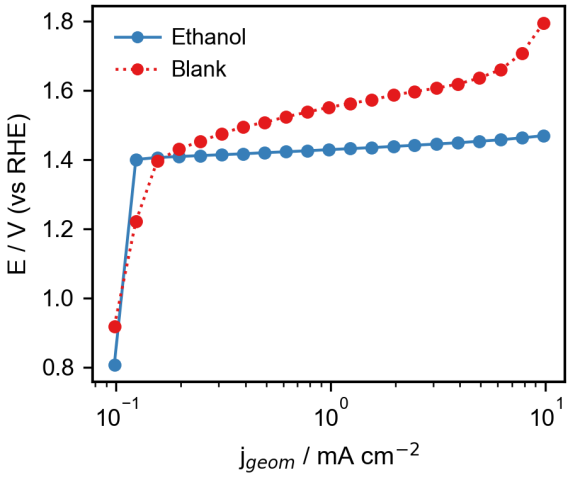

Figure S10. iR-corrected polarization curves for 1 M ethanol in 1 M NaOH (blue curve) and 1 M NaOH (red curve) using an electrode with only electrodeposited nickel. The lower potential recorded for the blue curve demonstrates the possibility of ethanol oxidation on nickel at about 1.4 V.

S12. Comparison of long-term stability of Pd-based catalysts for ethanol oxidation

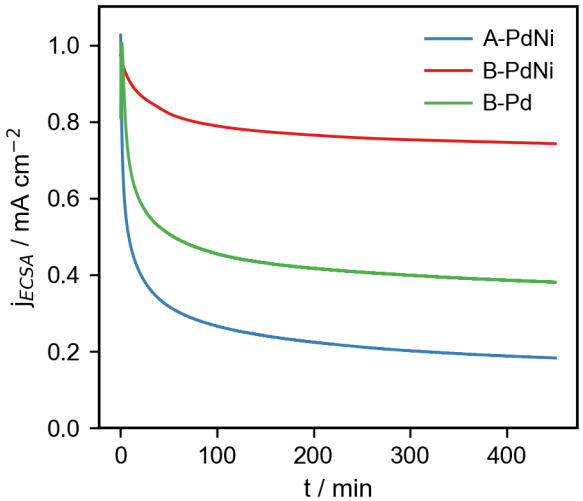

Figure S11. Long-term chronoamperometric curves (normalized by the ECSA) obtained using the three different Pd-based catalysts during ethanol oxidation (1 M ethanol in 0.1 M NaOH). Applied potential was +0.9 V and the total experiment time was 8 h.

S13. Voltammetric onset of 1 M ethanol oxidation in 0.1 M vs 1 M NaOH

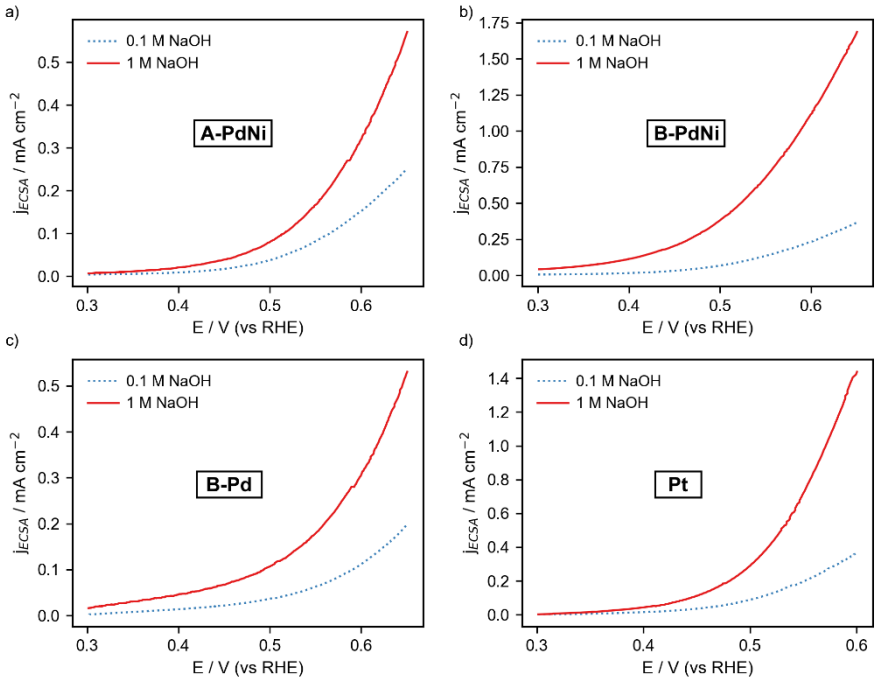

Figure S12. Voltammetric response normalized by the ECSA for 1 M ethanol oxidation using the different catalysts in a quiescent solution. Scan rate was 10 mV s^{-1}. Dashed blue line represent the response obtained in a 0.1 M NaOH solution while the solid red line represents the response obtained in 1 M NaOH. Since a significant iR drop distortion was observed at higher current densities, only the onset of the voltammetric process is shown where the iR drop is negligible and responses can be compared.

S14. Electro-oxidation of acetaldehyde with B-PdNi catalyst

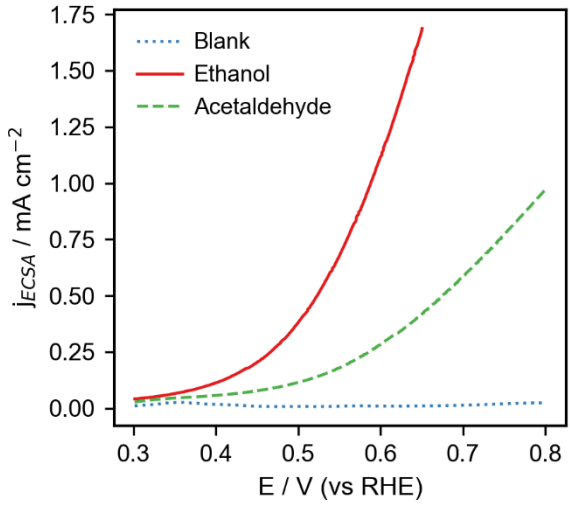

Figure S13. Voltammograms for oxidation of 1 M ethanol and acetaldehyde in 1 M NaOH using the B-PdNi catalyst. Blank voltammogram is also shown for comparison. Curves were normalized by the electrochemical surface area (ECSA) and potentials are referred to the reversible hydrogen electrode (RHE). Since a significant iR drop distortion was observed at higher current densities, only the onset of the voltammetric process is shown where the iR drop is negligible and responses can be compared.

S15. References

[1] J.D. Lović, V.D. Jović, Electrodeposited Pd and PdNi coatings as electrodes for the electrochemical oxidation of ethanol in alkaline media, J. Solid State Electrochem. 21 (2017) 2433–2441. https://doi.org/10.1007/s10008-017-3595-2.

[2] X. Niu, H. Zhao, M. Lan, Palladium deposits spontaneously grown on nickel foam for electro-catalyzing methanol oxidation: Effect of precursors, J. Power Sources. 306 (2016) 361–368. https://doi.org/10.1016/j.jpowsour.2015.12.044.

[3] J.-M. Kim, H.-T. Chung, Electrochemical characteristics of orthorhombic LiMnO2 with different degrees of stacking faults, J. Power Sources. 115 (2003) 125–130. https://doi.org/10.1016/S0378-7753(02)00709-7.